Scanning Electron Microscopy

Volume 1982
Number 1 *1982*

Article 26

1982

Electron Signal and Detector Strategy

L. Reimer
Universität Münster

Electron Beam Interactions With Solids (Pp. 299-310)
SEM, Inc., AMF O'Hare (Chicago), IL 60666, U.S.A.

ELECTRON SIGNAL AND DETECTOR STRATEGY

L. REIMER
Physikalisches Institut, Universität Münster, Domagkstrasze 75
D-4400 Münster, FRG
Phone No. 0251 83 3663

ABSTRACT

The scintillator-photomultiplier combination (Everhart-Thornley detector) for detecting secondary and backscattered electrons (SE and BSE) has the best properties concerning signal-to-noise ratio and bandwidth as compared to other detectors (semiconductor detectors or channel plates).

Two opposite Everhart-Thornley detectors A and B are proposed for a better and reproducible angular selection of the SE. The field strength at the specimen is reduced either by a grid or ring electrode to separate the SE with regard to their exit momenta. This offers the possibility to record the signals A, B, A+B, and A−B. The signal A+B shows material and channelling contrast and the signal A−B topography with a clear distinction of elevations and indentations. Furthermore, this signal A−B is proportional to dz/dx for tilt angles $\Phi = 0 - 60°$ and the surface profile can be recorded by analogue or digital on-line integration.

Backscattered electrons can be recorded optimally by using scintillators or a conversion of BSE to SE at plates covered with MgO. Multi-detector systems offer a determination of the specimen tilt Φ and azimuth χ which can be used for a surface reconstruction or in x-ray microanalysis for a ZAF-program of tilted surfaces. The signal A+B shows predominately material and channelling contrast and A−B the topography, however, with a worse resolution than the SE mode and with image artifacts like steps at flat interfaces between materials of different Z.

The electron-backscattering pattern (EBSP) shows advantages compared to an electron channelling pattern (ECP), and methods have been developed to record EBSPs and to use the shadow of the 'skyline' in an EBSP for a three-dimensional reconstruction of the specimen surface.

Energy-selection of the BSE and digital image processing will be further improvements for these imaging and recording techniques.

Keywords and phrases: Detectors, Backscattered electrons, Multi-detector systems, Secondary electrons, Material contrast, Topographic contrast, Channelling contrast, Magnetic contrast, Surface reconstruction, Recording, Electron-backscattering pattern, Energy-selection, Electron channelling pattern, Image processing.

INTRODUCTION

A conventional scanning electron microscope equipped with an Everhart-Thornley detector for SE (and a semiconductor for BSE) can make nice micrographs but it is not optimized to make the best use of the physics of electron-specimen interactions. The aim of a signal and detector strategy is a better angular and energy selection of the emitted particles and radiations but with a high collection efficiency to avoid a low signal-to-noise ratio. Furthermore the signals should be more quantitative to reconstruct e.g. the surface topography and the material composition.

In this paper we review some earlier work and experiments done recently in our laboratory for a better detector strategy of SE and BSE. We concentrate the discussion on those strategies which can be used more universally. In particular each contrast needs its own strategy and e.g. an effective collector for cathodoluminescence cannot be combined with a universal BSE and SE detection system. The discussed solutions will be examples only and shall demonstrate how a detector strategy can be realized with low expense and shall give impulses to users and manufacturers of SEMs to think more about modifications of detector systems.

The physics of electron-specimen interactions is summarized elsewhere (Reimer 1979) but the most important laws about SE and BSE emission will be repeated in the corresponding sections. Detector strategy depends on and is limited by the possibilities and the size of the detectors. Therefore, before the SE and BSE modes are discussed the most important detection systems will be summarized.

DETECTOR SYSTEMS

The scintillator-photomultiplier combination (Everhart-Thornley detector, ETD) with a positively biased grid for the collection of the SE is the most effective detector with a large band-width up to a few MHz and a low noise. The r.m.s. of the noise signal is only a factor 1.5 − 2 larger than the shot noise (Baumann and Reimer 1981)

$$N = [\, 2\, e\, I\, \Delta f \,]^{1/2} \qquad (1)$$

of an incident electron current I (Δf = band-width). There is no better detector for SE. However, the conventional ETD is a completely insufficient detector for BSE due to the fixed take-off angle and a very small solid angle of detection $\Delta\Omega =$

LIST OF SYMBOLS

a = Specimen-scintillator distance (cm)
A,B = Two opposite Everhart-Thornley detectors
c = Constant
C = Capacitance (F)
d = Distance (cm)
D = Detector area (cm^2)
E = Electron energy (eV)
E_p = Most probable energy (eV)
I = Incident electron current (A)
N = Noise signal
r = Radius of sphere (cm)
R = Electron range ($g\ cm^{-2}$)
R_{in} = Input-impedance of preamplifier (ohms)
S = Mean signal
U_v = Video signal
x = Coordinate in specimen plane
z = Coordinate parallel to the specimen normal
α_p = Electron probe aperture (rad)
β = Mean δ_{BSE}/mean δ_{PE}
γ = Value of γ-control unit
δ = Secondary electron yield
Δf = Band-width (Hz)
$\Delta\Omega$ = Solid angle of collection (detection) (sr)
η = Backscattering coefficient
Φ = Tilt angle
χ = Azimuth
ψ = Take-off angle
σ = Sum of η and δ
τ = Time constant (s)

$D/a^2 \cong 10^{-2} - 10^{-1}$ sterad ($D \cong 1\ cm^2$ = detector area, a = 5 – 10 cm = distance specimen-scintillator). With commonly used primary electron energies and potentials of the ETD, the BSE trajectories are little influenced by electrostatic collection fields and it is necessary to use a larger solid angle of collection.

Another possibility for BSE recording is the use of semiconductor detector with an internal amplification by electron-hole production on the order of $10^3 - 10^4$. Because of the large capacitance C of the depletion layers a low input-impedance R_{in} of the preamplifier has to be used to keep the time constant $\tau = R_{in} C$ small. Small R_{in} can be realized if the output current of the semiconductor detector is large due to a sufficient high electron probe current and/or if a large $\Delta\Omega$ with a high collection efficiency is used. Small C are obtainable by a small area of the detector and by increasing the width of the depletion layer by reverse biasing. Then a semiconductor can operate at television frequencies, otherwise the bandwidth is decreased $\cong$ 100 kHz if operating with low currents. A semiconductor offers no advantage as compared to a scintillator-photomultiplier combination. All typical applications for semiconductor detectors can also be solved with a scintillator on a light-pipe.

Both scintillation and semiconductor detectors show a signal (number of light quanta and electron-hole pairs respectively) which is proportional to the BSE exit energy and which shows a threshold energy E_{th} on the order 1 – 10 keV caused by the absorption of electrons in a conductive metal coating or a dead layer. This means that BSE with a large exit energy contribute to the signal with a larger amplification $\propto (E - E_{th})$.

Channel plates (see e.g. Griffiths et al. 1972) convert the BSE to SE which are multiplied by a repeated SE emission in an array of small tubes of $\cong$ 50 μm like in a photomultiplier but with a continuous voltage drop along the conductive tube walls. The signal will be proportional to the SE yield, that is $\propto E^{-0.8}$ for BSE energies $\geq$ 1 – 2 keV. They are excellent detectors for single particle counting and can be used to select also the position of incidence (position-sensitive detector). However, they only work with a limited number of counts, and the high electron density in SEM demands that the system has to work in an analogue mode without resolving single counts. The bad vacuum condition in an SEM and the frequent vacuum interruptions also cause a stronger contamination especially at the end of the tubes. Therefore, channel plates may be of interest for special applications but are no alternative to scintillators or semiconductors. With a fluorescent screen at a positive high-voltage a channel plate can be used as an image intensifier (Venables et al. 1974).

Another possibility is the conversion of BSE to SE and the collection by an ETD (Moll et al. 1978, Reimer and Volbert 1979, 1980a). Fig. 1 shows an arrangement for high and low take-off angles. The converter plate of copper on resin is coated with MgO as a substance of high SE-yield δ. But because it is an insulator, the sum $\sigma = \eta + \delta$ of the backscattering coefficient η and the SE-yield δ cannot become larger than 1. This would introduce a positive charging which prevents further SE from leaving the converter plate. Therefore, the BSE/SE conversion coefficient is independent of the BSE energy and decreases at energies $\geq$ 20 – 30 keV when σ becomes < 1. BSE/SE conversion is also present every time at the pole-piece and other parts of the specimen chamber. However, on metals the SE-yield decreases $\propto E^{-0.8}$ with increasing BSE energy. The action of the BSE/SE conversion can be switched on and off using an earthed grid $\cong$ 3 mm in front of the converter plate and by a negative or positive bias of the converter plate respectively.

DETECTOR STRATEGY FOR THE SE MODE

Contributions to the SE signal

The SE emission shows the following characteristic effects (Reimer 1979):

1. The secondary electron yield δ for normal incidence ($\Phi = 0$) consists of a contribution δ_{PE} by the primary electrons concentrated on the area of the electron probe and an exit depth of 1–10 nm, a contribution δ_{BSE} produced by BSE on their trajectories through the exit depth and an external contribution δ_{ext} by SE emitted by BSE in the specimen chamber especially at the pole-piece:

$$\delta = \delta_{PE} + \delta_{BSE} + \delta_{ext} = \delta_{PE}(1 + \beta\eta) + \delta_{ext} \qquad (2)$$

The mean contribution of a BSE to δ is a factor $\beta \cong$ 2–3 larger than the contribution δ_{PE} due to the lower energy of BSE than of PE and the longer path inside the exit depth (Drescher et al. 1970 , Reimer and Drescher 1977). The SE yield increases with increasing Z due to the increase of the backscattering coefficient η in (2), but δ also depends on the specimen contamination and work function, and the increase with

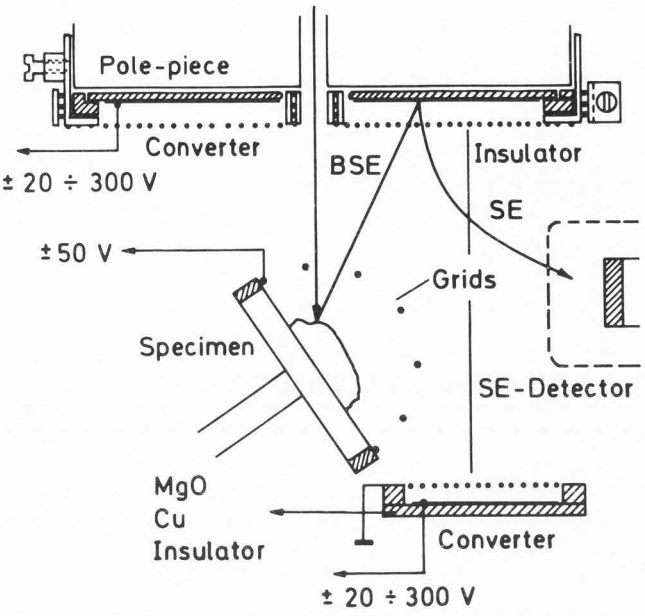

Fig. 1. BSE/SE converter plate for high and low take-off angle collection of BSE emitted at an inclined specimen.

increasing Z is less pronounced than the backscattering coefficient. The SE yield shows a maximum for primary electron energies in the order of a few hundreds eV. For $E \geq 1$ keV the SE yield is proportional to the probability of ionization, that is $\propto \ln E/E$ (Bethe law) which can be approximated by $\propto E^{-0.8}$ (Reimer 1973).

2. On polycrystalline surfaces, δ increases with increasing tilt angle Φ : $\delta_{PE} \propto 1/\cos \Phi = \sec \Phi$. δ_{BSE} also increases with increasing Φ but the sum $\delta_{PE} + \delta_{BSE}$ shows systematic deviations from a $1/\cos \Phi$-law dependent on the atomic number Z (Drescher et al. 1970).

3. The energy distribution of SE consists of a most probable energy $E_p \cong 2$–5 eV and all electrons with $E \leq 50$ eV are called SE by convention.

4. On polycrystalline surfaces, the angular distribution is proportional to sin ψ (ψ = take-off angle, $\psi = 90°$ for normal take-off) independent of energy, tilt angle and material.

5. Only the contribution δ_{PE} contributes to the high resolution with an information depth of a few nm whereas the contribution δ_{BSE} (+ δ_{ext}) caused by the BSE shows an exit depth and lateral spread on the order of half the electron range R (see contribution to the BSE signal, below). At edges and small particles the SE yield increases due to the larger escape probability of the BSE.

6. The SE yield depends on crystal orientation (work function and channelling effect, see above) but the variations are smaller than for BSE (Reimer et al. 1971).

7. The Lorentz force of external stray fields influences the SE trajectories and an angular selection of SE momenta results in the magnetic contrast type-1. The influence of electrostatic stray fields and the specimen bias result in the potential contrast.

If all emitted SE are collected by the ETD the signal only depends on the inclination of the local surface normal to the electron beam (tilt angle Φ) and all normals lying on a cone with the angle Φ and the beam as a cone axis show the same signal independent of the azimuthal angle χ of the surface normal. A further contribution to the SE signal is the enhanced emission at edges. This edge effect makes an SE image sensitive to small surface irregularities which appear as bright spots. But these effects offer no possibility to get an unambiguous interpretation of surface topography. E.g. it is not possible to distinguish surface elevations or indentations. This needs more shadows in the image which means that surfaces with their normal in an opposite direction to the detector should appear darker.

Computed SE trajectories show that the collection field of the ETD cannot be sufficient to collect all SE, especially SE with exit momenta in the opposite direction to the detector end on the pole-piece. However, this type of selection of exit momenta cannot be controlled quantitatively and depends on the working distance and the position of the beam on the specimen stub. The latter results in a gradient of the mean signal across the stub.

E.g. the magnetic contrast type-1 is a mode which depends very sensitively on the angular selection of SE. The optimum signal variations $\Delta S/S \cong 1$–10% are obtained if only half of the emitted SE are collected. The small $\Delta S/S$ needs a black-level subtraction, and this type of contrast can be observed only in a small zone of the specimen with a width of $\cong$1mm due to the gradient of the mean signal S across the specimen stub.

Proposals for a detector strategy of SE

From the discussion of the contributions to the SE signal we can declare the following aims of a detector strategy for SE:

1. More controlled and reproducible selection of SE exit momenta.

2. More uniform selection and a constant mean signal across the specimen stub.

3. Suppression of the BSE contribution δ_{ext} to the SE signal at the pole-piece.

4. Simultaneous record of a BSE image and subtraction to eliminate the BSE contribution δ_{BSE} to the SE signal.

5. Multiple detector systems for separating different types of contrast by A + B sum or A − B difference signals and for an analogue or digital reconstruction of the surface topography.

6. Use of retarding field or an electrostatic prism spectrometer for measuring the surface potential or the SE energy spectrum.

7. A detector system shall not influence the free space for other detection modes, e.g. BSE or x-ray.

An earlier attempt to select take-off angles of the SE emission and to make the signal more uniform across the specimen stub is reported by Banbury and Nixon (1969). Their detector consists of additional cylindrical electrodes with an opening directed to the ETD and covered with a grid and of a plane top electrode. The electrodes can be operated with different biases, and the SE trajectories can be influenced like a fountain. This detector was applied to influence the dependence of the signal on the surface potential for potential contrast and to increase the magnetic contrast type-1 caused by

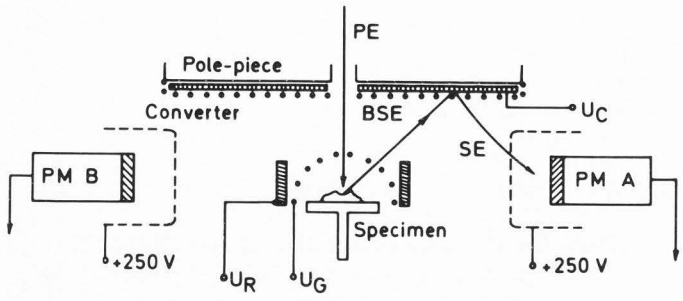

Fig. 2. Two-detector system for A, B, A+B and A−B imaging with SE (converter plate below the polepiece positively biased, grid or ring electrode a few volts positive) or with BSE (converter negatively biased, ring or grid a few volts negative). PM = photomultiplier, U_C, U_R, U_G = biases of converter plate, ring and grid.

magnetic stray fields (Gentsch and Reimer 1972). It is a disadvantage of this device that the electrodes are sources of SE when struck by the BSE and an uncontrollable part of this BSE/SE conversion contributes to the image, and using one ETD the selection of exit momenta is only possible in one direction. Especially this device does not fulfill aim (7) above.

A two-detector system for SE and BSE

Therefore, we used the arrangement of Fig. 2 with two opposite ETDs (Volbert and Reimer 1980). The spherical grid over the specimen (a few wires only so that the primary beam can pass the grid) or as an alternative a ring electrode around the specimen stub have the aim to decrease the electric field normally caused by the grid in front of the ETD and which is needed as a collection field for SE. Then the SE first can move on nearly straight trajectories due to their exit momenta and are collected by the two ETDs after passing the grid or after entering the collection field behind the ring electrode. This arrangement fulfills aims 1–5 and 7 above.

The suppression of the external contribution δ_{ext} (aim 3) excited by BSE at the pole-piece and other parts of the specimen chamber can be realized by the converter plate with an earthed grid and a positively biased converter plate acting as an electron trap. In this mode a converter plate even shows an advantage for the SE mode if it is switched off. A further reduction of δ_{ext} results with a carbon coated ring around the specimen stub, which absorbs all BSE which do not strike the BSE/SE converter.

For realizing aim 4 a BSE signal can be recorded simultaneously or by a second record and can be subtracted from the SE signal analoguely or digitally respectively. Scintillation detectors can be used to record a BSE signal and a conventional SE image simultaneously (Volbert 1981). Another possibility for using the BSE/SE converter is the switching off and on of the converter with a frequency of a few 100 kHz and separating the signals behind the photomultiplier with a gate amplifier. A problem of recording the difference signal $S_{SE} - k\, S_{BSE}$ is that each BSE image shows a selection of emission angles and of BSE energies and that this selection does not correspond exactly to that one which is responsible for the δ_{BSE} contribution to the SE signal. BSE effects in SE

Table 1. Enhancement (+) and suppression (−) of different contrasts in the A+B and A−B SE and BSE modes.

Contrast	A+B SE	A−B SE	A+B BSE	A−B BSE
Topography	no shadows	+	−	(+) artifacts!
Material (Z)	+	−	+	−
Channelling	+	−	+	−
Magnetic type-1	−	+		

micrographs will be suppressed by this method but surely cannot be eliminated completely.

The two simultaneous SE signals A and B offer the possibility of recording the single A or B SE micrographs, or using an operation amplifier the signals A+B and A−B+C can modulate the CRT (cathode ray tube: C = constant background to record also 'negative' values of A−B). Table 1 shows how the A−B and A+B signals enhance (+) or suppress (−) the different contrast effects.

Examples for the separation of topography and material contrasts are shown in the micrographs (Fig. 3) of a glass matrix with zirconium oxide inclusions (bright in material contrast in the A+B SE mode). This material contrast vanishes and a real topography appears in the A−B SE micrograph. The micrographs of an integrated circuit (IC) (Fig. 4) as an example for well-defined surface steps show that the A+B micrograph cannot distinguish between opposite surface steps whereas this is possible in the A−B SE mode and there are no difficulties to distinguish surface elevations and indentations. Small particles (dust) which appear bright in the A, B or A+B mode due to the diffusion of BSE out of the particle show shadows in the A−B SE micrograph but are more reduced in contrast. If the electron beam hits the centre of the particle SE are emitted by the BSE on both sides and A−B=0. The corresponding BSE micrographs in Figs. 3 and 4 will be discussed later.

Examples for separating the channelling contrast of polycrystalline metal specimens and the topographic contrast at the grain boundaries are already published (Volbert and Reimer 1980, Hoffmann and Reimer 1981). The aim 2 of detector strategy can optimally be demonstrated with the magnetic contrast type-1 which becomes uniform in the A−B SE mode over the whole specimen stub.

Reconstruction of surface topography

The dependence of the A−B SE signal on the tilt angle Φ and azimuth χ can be used to record directly a signal proportional to dz/dx (z = coordinate parallel to the electron beam, x = parallel to the connection of the two detectors A and B in Fig. 2). This shall be evaluated by using Fig. 5a which shows the emission characteristics of SE approximately proportional to sin ψ and sec Φ.

$$\frac{d\delta}{d\Omega} = \frac{\delta_0}{\pi} \sin\psi \sec\Phi\,;$$

$$\int \frac{d\delta}{d\omega}\, d\Omega = \int_0^{\pi/2} \frac{d\delta}{d\Omega}\, 2\pi\cos\psi d\psi = \delta_0 \sec\Phi \qquad (3)$$

(δ_0 = SE emission for normal incidence, $\Phi = 0$) and by Fig. 5b which shows the angles Φ and χ of the surface normal N and the direction E of the electron beam on a unit sphere. The shaded part of the emission characteristics in Fig. 5a will contribute to the SE signal δ_B of detector B. This corresponds to the shaded area on the unit sphere in Fig. 5b. For calculating δ_B the distributing (3) has to be integrated over the shaded area:

$$\delta_B = \frac{2\,\delta_0}{\pi} \sec\Phi \int_0^{90-\Phi_x} \int_0^{\chi'} \sin\psi\cos\psi \, d\psi d\chi \qquad (4)$$

Spherical trigonometry results in $\sin\Phi_x = \sin\Phi\cos\chi$ and $\cos\chi' = \mathrm{tg}\psi\,\mathrm{tg}\,\Phi_x$. Substitution in (4) results in

$$\delta_B = \frac{\delta_0}{2} \sec\Phi\,[1 - \sin\Phi_x]$$

$$\delta_A = \frac{\delta_0}{2} \sec\Phi\,[1 + \sin\Phi_x]$$

$$\delta_A + \delta_B = \delta_0 \sec\Phi$$

$$\delta_A - \delta_B = \delta_0 \sin\Phi_x \sec\Phi$$

$$= \delta_0\,\mathrm{tg}\,\Phi\cos\chi = \delta_0 \frac{dz}{dx} \qquad (5)$$

The latter relation shows that the difference signal A – B is proportional to dz/dx and if x is parallel to a linescan an analogue integration can directly record the z-profile of the specimen. Fig. 6a demonstrates by a linescan across the centre of a sphere that the A – B signal is proportional dz/dx which corresponds to $\propto x/(r^2-x^2)^{1/2}$ (r = radius of the sphere) up to $\Phi = 60°$. This method will not have the accuracy of stereometry but it can be a method to get an on-line record of the surface topography if the integrated A – B signal is recorded in Y-modulation on the CRT. However, each linescan starts at the level z = 0 if no information about the surface slope in the y-direction can be obtained by other methods. First experiments on model surfaces of known geometry show that this method works.

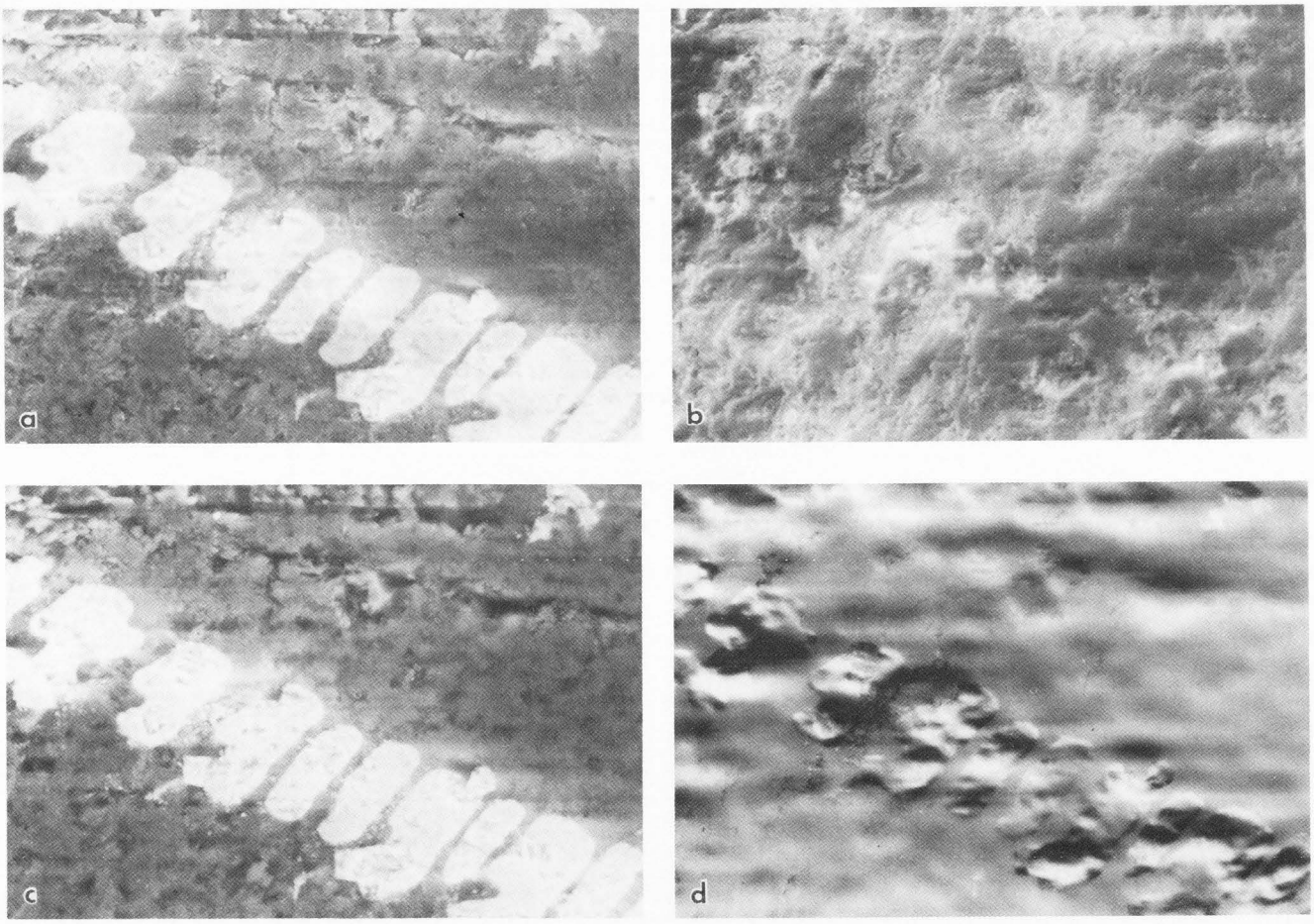

Fig. 3. Zirconium-oxide inclusions in a glass matrix, imaged in a) A + B SE, b) A – B SE with topographic contrast, c) A + B BSE mode, a) and b) with predominate material contrast. The d) A – B BSE mode shows a 'topography' which is an image artifact. (Horizontal field width: 100 μm)

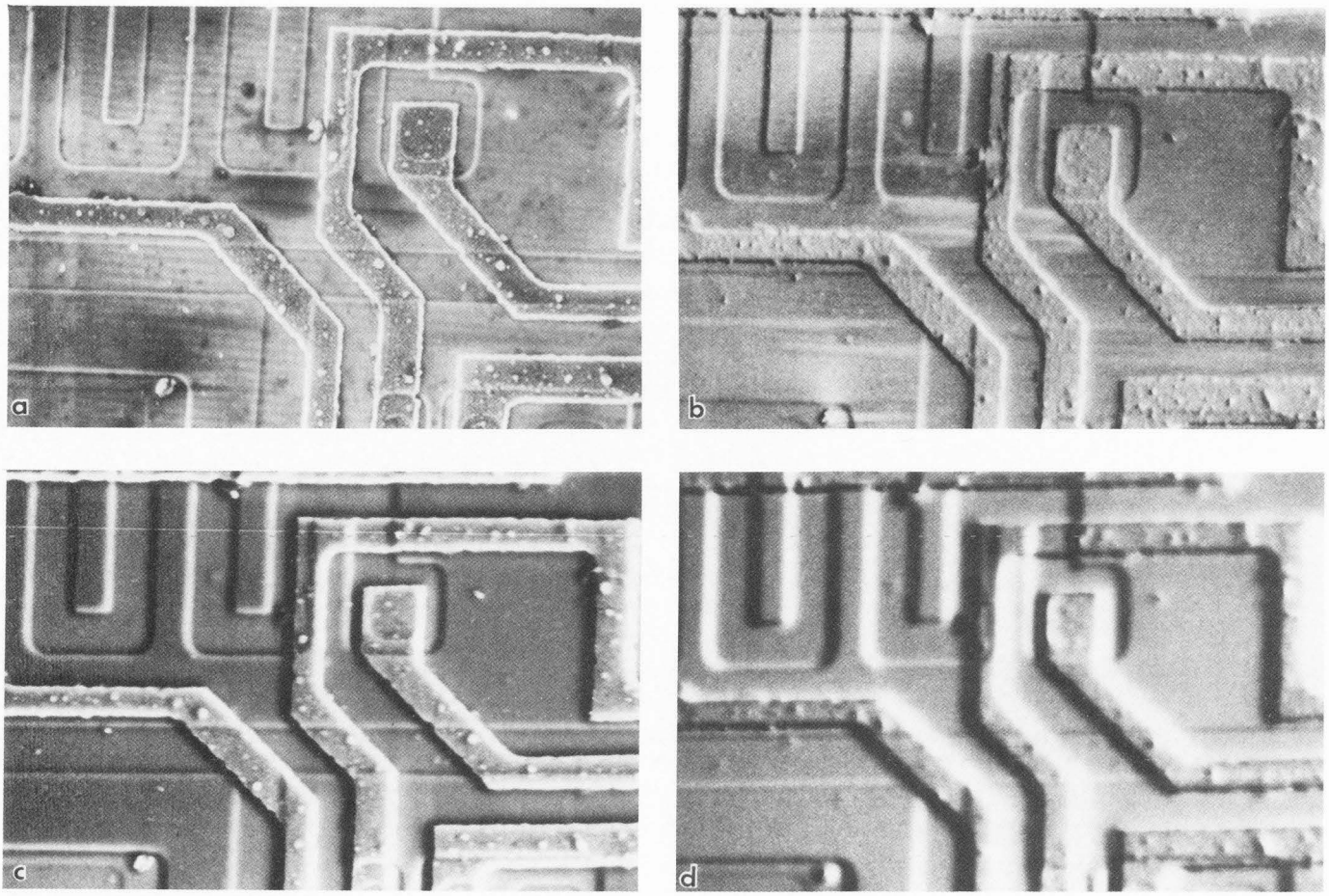

Fig. 4. Integrated circuit demonstrating the imaging of surface steps and small particles (dust) by the a) A SE, b) A – B SE, c) A BSE and d) A – B BSE modes. (Horizontal field width: 160 μm)

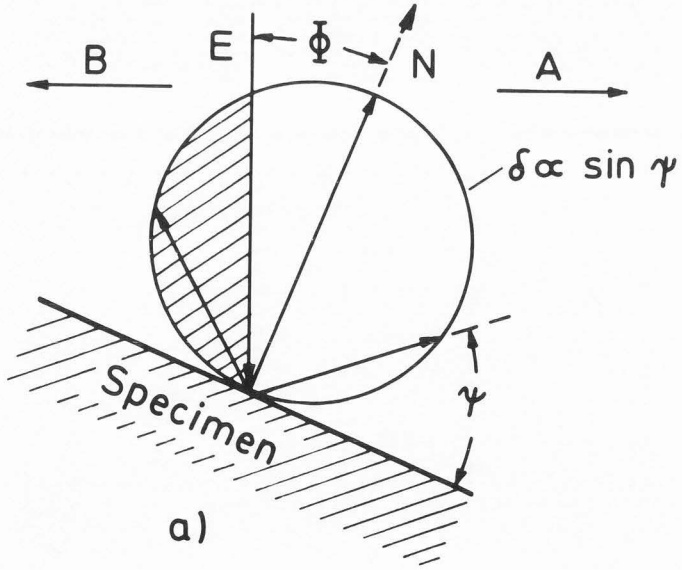

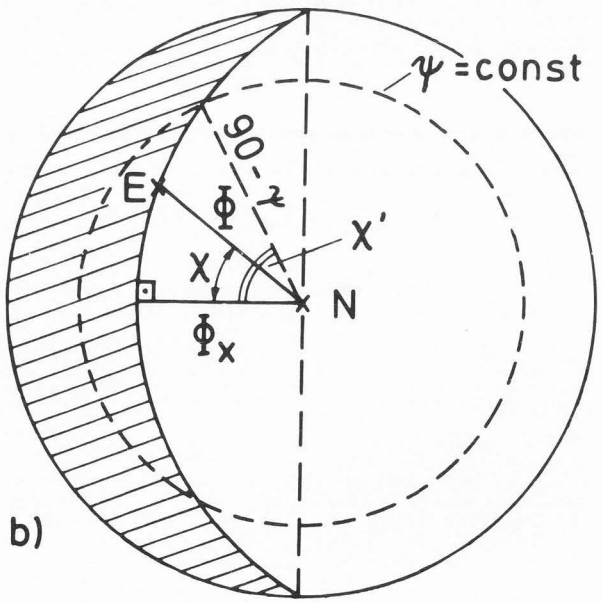

Fig. 5. a) Angular characteristics of SE emission at a specimen with a tilt angle Φ, ψ = take-off angle of SE, b) Angles on a unit sphere to calculate the fraction (shaded) of SE which are collected by the SE detector B on the left side. E = electron incidence, N = surface normal.

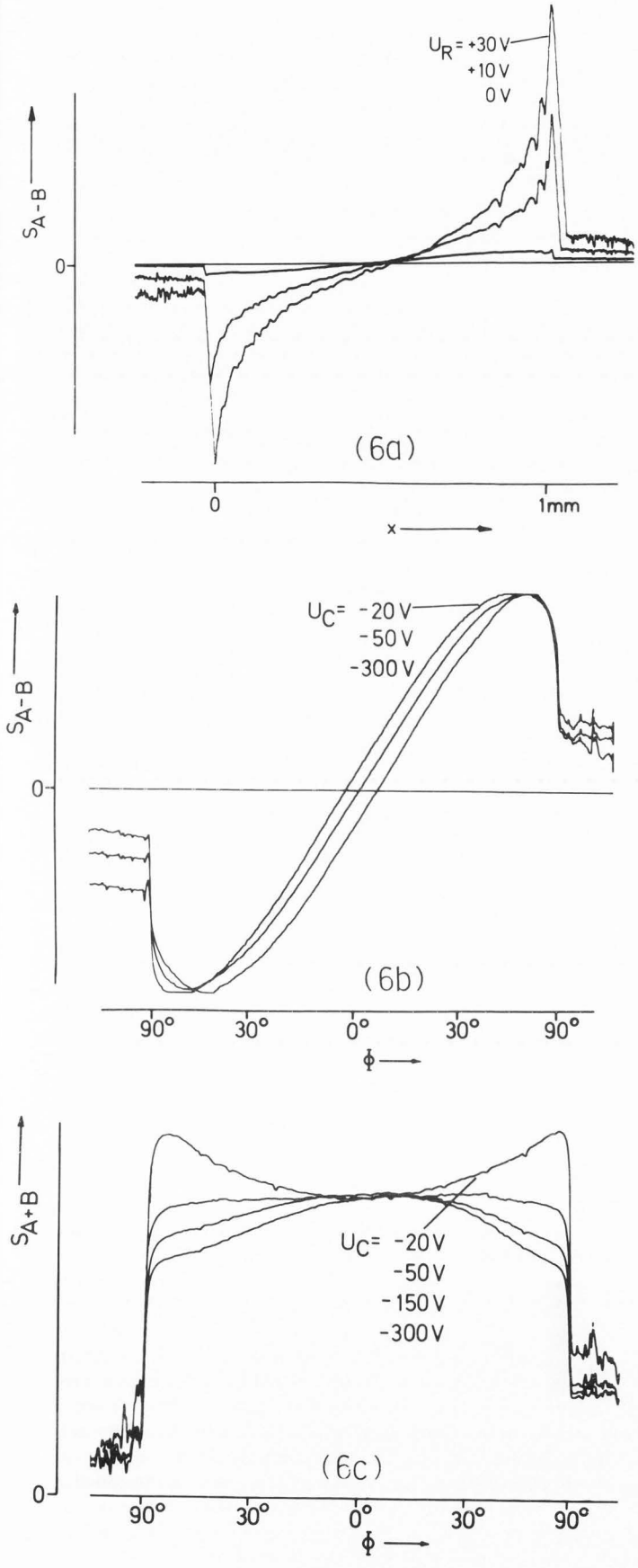

DETECTOR STRATEGY FOR THE BSE MODE

Contribution to the BSE signal

The BSE show the following interaction effects (Reimer 1979, Niedrig 1978):

1. The total backscattering coefficient η for normal incidence ($\Phi = 0$) increases continuously with increasing Z, and for minerals and alloys we recently confirmed the rule of Castaing (1960)

$$\eta = \sum_i c_i \eta_i \qquad (6)$$

(c_i = mass concentrations and η_i backscattering coefficients of the elements) as a best fit to experimental results. η is approximately independent of the incident electron energy E in the range E = 5–100 keV, but varies only between 0.2 and 0.3 for E = 1 keV (Reimer and Tollkamp 1980).

2. η increases with increasing tilt angle Φ.

3. The energy distribution shows a most probable energy ranging from 0.5 to 0.95 E. The most probable energy is shifted to E when increasing Φ.

4. The angular distribution is approximately $\propto \sin \psi$ for normal incidence but shows a reflexion-like maximum for oblique incidence.

5. The exit depth and lateral spread of the BSE is on the order of half the electron range $R \cong 6.7\ E^{1.66}$ (R in $\mu g\ cm^{-2}$, E in keV). The interaction volume decreases by energy filtering and using 'low-loss electrons'. At edges the BSE emission increases due to the increased probability of escape.

6. η depends on crystal orientation (channelling effect). Rocking the electron beam causes a variation of the total BSE yield on the order of $\Delta\eta/\eta$ = 5–10% for E = 10 keV which decreases with increasing E (Reimer et al. 1971, Drescher et al. 1974). This can be recorded as a channelling pattern (ECP) (Booker 1970). The channelling effect also modulates the angular distribution, which shows Kikuchi bands with a stationary electron beam (electron-backscattering pattern, EBSP) (Venables and Harland 1973). These channelling effects are concentrated on the mean penetration depth of the primary Bloch wave field on the order of a few nanometers only.

7. The Lorentz force of internal magnetic fields acts on the BSE trajectories resulting in variation of < 1% depending on the direction of $\hat{B}$. This effect increases $\propto E^{1.5}$ with increasing E.

The interaction effects 1-4 cause a superposition of material and topographic contrast which depends on the take-off direction of the BSE detector. Pronounced material contrast is observed for large take-off angles, and it is stronger than for the SE mode. Whereas the low-energy SE can be collected by a positively biased ETD, the BSE travel on straight

Fig. 6. Linescans across a sphere (1 mm steel ball), x = coordinate across the centre of the sphere) in the a) A − B SE mode, signal $\propto dz/dx \propto x/(r^2 - x^2)^{1/2}$, b) A − B BSE mode, signal $\propto x = r \cos \Phi$ and c) A + B BSE mode with voltages U_c of the converter plate which result in uniform contrast independent on x and optimum for material contrast.

lines to the detector. This causes sharper shadow effects if imaging a surface topography at low take-off angles and if using a detector with a small solid angle of collection $\Delta\Omega$. These effects can only be applied successfully if the take-off angle of the BSE can be varied by turning a semiconductor or scintillator to different take-off positions. A small $\Delta\Omega$, however, decreases the signal-to-noise ratio. An optimum has to be found to get a sufficient signal-to-noise ratio (large $\Delta\Omega$) and a limitation of the selected angular range (small Ω). For large tilt angles Φ and low take-off angles at the reflexion-like maximum a contrast reversal of material contrast can be observed (Reimer et al. 1978).

Proposals for a detector strategy of BSE

A BSE detection system which makes the best use of electron-specimen interactions shall have the following properties:

1. Different BSE detectors with a large solid angle of collection at low and high take-off angles to get pronounced material or topographic contrasts.
2. Detectors variable in the take-off angle to work with optimum contrast for different types of contrast.
3. Uniform material contrast independent of the tilt and azimuth of the surface normal to get a quantitative signal for measuring the mean atomic number $\overline{Z}$.
4. Two or four BSE detectors for a quantitative determination of the tilt angle Φ and the azimuth χ.
5. Recording of an EBSP and the 'skyline' (see below) of the specimen.
6. Energy-filtering of BSE ('low-loss electrons') to get a better resolution and contrast.
7. If possible the detector system shall not influence the free space for other detectors.

Not all possibilities of BSE recording can be realized with one detection system, and depending on the information wanted different detector systems have to be applied.

For realizing point 1 several authors used scintillators near the specimen mounted on an elongated light pipe of the ETD system (Blaschke and Schur 1972, Wells 1974). Contrary to the conventional BSE mode of an ETD solid angles of collection $\Delta\Omega$ of a few sterad are obtainable. A flat scintillator below the pole-piece shows the advantage of a more uniform collection of the BSE scattered in large angles $> 90°$ and will be optimum for evaluating material contrast (Robinson 1975). Another possibility is to use the conventional SE mode and a high and low take-off BSE/SE conversion by switching on and off the converter-grid combinations in Fig. 1 (Reimer and Volbert 1979). Though BSE are converted to SE at the whole plate below the pole-piece the largest fraction of the SE signal is collected from an area between specimen and ETD and a reduced fraction from the side and backward areas. For an optimization it will be necessary to calculate SE trajectories from the specimen and the converter plate to the ETD. For material contrast it is also useful to work with the A + B BSE signal of the two-detector system of Fig. 2 (see below and Fig. 3c)

A BSE/SE conversion can also be realized by a transparent metal foil in front of the ETD, and the SE are recorded which are generated by the transmitted BSE (Walker and Booker 1976). This arrangement has the advantage of realizing a rough high-pass energy selection if the thickness of the foil is only a small fraction thinner than the range of the primary electron energy. Then, slow BSE will be absorbed in the foil. The method will be of interest for the magnetic contrast type-2 and the channelling contrast which both show the largest contrast contribution from the low-loss electrons. However, the foil thickness has to be adapted carefully for the electron range to get an optimum BSE/SE conversion.

Detectors with a variable take-off angle (point 2) have the advantage of getting optimum signals for magnetic contrast type-2, material and topographic contrasts. They can either consist of a semiconductor detector (Wells 1978, 1979) or a scintillator disc mounted at a bent light pipe so that the scintillator turns eccentrically around the specimen when the light-pipe cylinder rotates (Reimer et al. 1978).

Material contrast can be used to distinguish different phases. A quantitative use (point 3) needs an independence of the BSE signal on the tilt angle Φ of the surface. Fig. 6c shows signals across a sphere using a BSE/SE converter below the pole-piece with two ETDs (Fig. 2) and recording the sum A + B. Conditions can be found which show approximately uniform signals. A histogram of the data from a digital scan contains peaks from different phases (Fig. 7). A calibration with a material of known Z and η (e.g. Cu) is needed to transform the scale of signal amplitude to a Z-scale. This offers the possibility of getting quantitative mean atomic numbers $\overline{Z}$ or $\overline{\eta}$ for the ZAF correction of x-ray microanalysis. This technique can be applied for all types of high take-off angle BSE detectors but the signal has to be calibrated because the differences in the efficiency versus BSE energy cause different calibration curves for the Z versus BSE signal.

An absolute, standardless method for measuring η needs the electron current, and the backscattered current should not be falsified by backscattering at the collector to the specimen and by SE excited at the collector. Therefore, an exact measurement of η is only possible with a spherical collector and a grid in front of it to prevent the SE emission of the collector (Reimer and Tollkamp 1980).

The accuracy for the determination of $\overline{Z}$ depends on the signal-to-noise ratio but cannot be increased by increasing the electron probe current and/or the recording time because the surface topography, contamination layers and channelling contrast influence the backscattering coefficient. This results in estimated accuracies $Z \pm 2$ for low and $Z \pm 5$ for high atomic numbers.

Multi-detector system for BSE

Two BSE semiconductor detectors were first used by Kimoto et al. (1966). They showed that the sum A + B results in material and the difference A − B in topographic contrast. This technique can also be applied with the BSE/SE converter system of Fig. 2 or with a slided scintillation disc below the pole-piece and two ETDs (Reimer and Volbert 1980). However, though the A + B BSE signal has a large advantage to get more quantitative material contrast, the difference signal A − B has to be used with care and criticism. The resolution of the BSE signal is worse than the SE signal and e.g. A − B BSE micrographs of a surface step (e.g. conductive lines of an IC in Fig. 4) show a more trapezoid-like profile than the more realistic A − B SE micrograph. This lack of

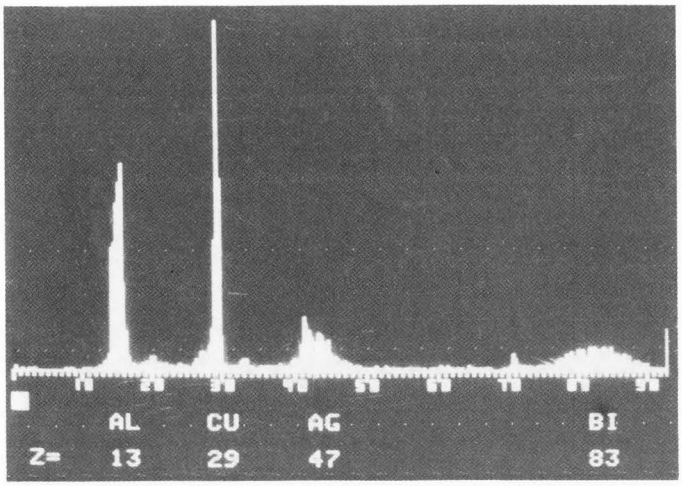

Fig. 7. Histogram of the A + B BSE mode for a four-element specimen of Al, Cu, Ag and Bi calibrated to a Z-scale.

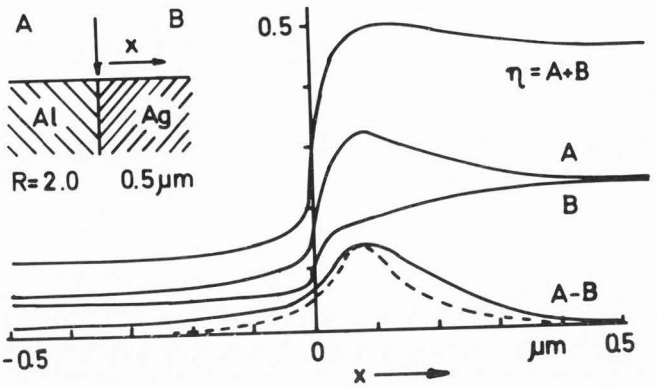

Fig. 8. Monte-Carlo calculation (20 keV) of the contributions to detectors A and B demonstrating the artificial contrast of the A – B signal at the interface between Al and Ag (R = practical ranges). (Dotted line: signal $\propto (E - E_{th})$ with $E_{th} = 10$ keV).

resolution can also be seen in Fig. 3d and is caused by the electron diffusion and the increased exit area and information volume of the BSE. This effect also produces a 'surface step' as an image artifact if a flat boundary of low and high Z materials is imaged (Reimer and Volbert 1980b). With Al on the left and Ag on the right electrons backscattered in Ag can pass the Al with a low density and low Z. More electrons are collected, therefore, by detector A and the signal increases like at a pure Ag edge. Because this is reversed for Ag on the left and Al on the right, the A – B signal results in a step-like contrast. This can be confirmed by Monte-Carlo calculations (Fig. 8). Fig. 2 in Volbert and Reimer (1980) shows this effect for a lamellar eutectic Al-Ag alloy. Using E = 20 keV it looks like the Ag lamellae are higher than the Al lamellae, whereas the surface looks quite different if using E = 5 keV electrons with a reduced penetration depth, because then the real surface of the mechanically polished specimen is imaged. The A + B BSE signal at 5 keV shows the distribution of Al and Ag at the surface, and the A – B BSE signal a correct surface topography which does not differ from an A – B SE micrograph. Also the A – B BSE signal in Fig. 3d shows artificial topographic contrast at the boundaries between the zirconium oxide and the glass matrix which cannot be observed in the A – B SE micrograph (Fig. 3b).

Though the A – B BSE mode does not offer an advantage in imaging the surface topography, signals of a multi-detector system can be used to determine quantitatively the direction of the surface normal (tilt Φ and azimuth χ). This will be important for quantitative x-ray microanalysis (see *signal processing* below).

The use of four semiconductor detectors is proposed by Lebiedzik and White (1975) to calculate the direction of the surface normal with the aim of reconstructing the surface topography. In another version (Lebiedzik 1979) only two semiconductors are used to record the surface profile along the scan direction. We are testing a pyramid of scintillators over the specimen which is coupled to two photomultipliers. Either one or both sides of the pyramids can be recorded by using a shutter in the light pipe. It is necessary to fit the signals as a function of Φ and χ by an analytical formula. We used e.g. a steel ball of 1 mm diameter containing all directions of surface normals and recorded equidensities or fed the data from a digital scan into a minicomputer. Conditions can be found so that the A – B BSE signal is proportional to $\sin \Phi \cos \chi$ over a large angular range, that is proportional to x in a linescan across a sphere (Fig. 6b).

The detector strategy for BSE uses in all applications the model of straight trajectories of the BSE after leaving the specimen. Therefore, a channel plate or fluorescent screen observed by a television camera can be used beside the specimen as a multi-element direction-sensitive detector (see also recording of EBSP below). The BSE produce on the screen not only the EBSP but also a shadow of the specimen structure with the point of electron impact as a projection centre. This projected image is like a 'skyline' seen from this centre. E.g. a particle can be projected with the electron beam behind it and its height and profile can be calculated. Further possibilities shall be demonstrated by the following example. If you move with a car along a mountain-chain and take photographs of the skyline you can reconstruct the height and positions of the peaks by applying stereo-photometry. Furthermore the trace of one peak on the sky (screen) will be a height-profile of your road (electron trace of linescan on the surface). The sensitivity increases when the distance of the beam and the 'peak' decreases, and it will be useful to use structures of the specimen itself though it will be possible to put e.g. a needle near the specimen structure. If a minicomputer stores only the profile (skyline) for one point a lot of profiles for other points can be stored and computed.

Recording of ECP and EBSP

Semiconductor and scintillation detectors above the specimen can be used to record an electron channelling pattern (ECP) when rocking the electron beam. Disadvantages of this technique are:

1. A limited range of rocking angle ±(5–8°) which results in difficulties of indexing if the ECP does not contain low-indexed poles of Kikuchi bands.

2. The need for a small electron-probe aperture $\alpha_p \geq 10^{-4}$ rad ($\cong 10^{-2}$ rad for the normal SE mode) which reduces the maximum probe current and increases the probe diameter.

3. The shift of the electron probe on a caustic figure of a few μm diameter during rocking caused by the spherical aberration.

Advantages are:

1. The overlap of surface structures and ECP if defocusing the pivot point of rocking.

2. The direct record on the CRT of the SEM and the possibility to apply signal-processing.

In contrast, electron back-scattering patterns (EBSP) have the following corresponding advantages and disadvantages:

1. Large recorded angular range $\pm(30\text{–}50°)$ depending on the size of the screen and its distance from the specimen. The screen can be positioned horizontally to record EBSP at oblique incidence inside the reflexion-like maximum of BSE emission or vertically to record BSE scattered around 90° which shows low but more uniform intensity.

2. Use of large probe apertures α_p without influencing the EBSP quality. This allows one to work either with a high-current mode (low resolution) or the usual high-resolution mode in the order of $\cong$ 10 nm or better if using a field emission gun.

3. Recording of the pattern with a fixed electron beam.

4. Selection of the beam position with a scanned image. Changes of the EBSP can be observed if slowly scanning the beam over the specimen.

5. Recording of an EBSP on a film camera inside an SEM (Fig. 9) or observation of a fluorescent screen with a television camera. EBSP and image can be recorded on different CRTs simultaneously.

For both ECP and EBSP it is necessary to have a clean, contamination-free surface without a large crystal lattice distortion, e.g. by mechanical polishing. It is very effective to remove oxide and contamination layers and the Beilby-layer by ion-etching (Hoffmann and Reimer 1981). Many failures in applying these techniques can be attributed to a contaminated surface.

A quantitative determination of crystal orientation from EBSP is possible by using the projection of three balls in front of the screen (Venables and bin-Jaya 1977).

Energy-filtering

The value of an energy-filtering has been demonstrated using low-loss electrons with energy losses $\Delta E \geq 10\text{–}100$ eV for the decrease of the information depth and an increase of resolution (Wells 1971, 1972, 1979) and for the increase of contrast to observe single dislocations (Morin et al. 1979). Because the number of low-loss electrons is small, the detection system needs a large solid angle of collection and a high energy resolution. This can be solved only by a retarding field electron spectrometer with spherical grids. The large space of such a filter does not allow one to use this system in a concept which considers all the points of detector strategy listed above.

Otherwise electron spectrometry in SEM is not limited to low-loss imaging. It can offer further information, e.g. the local spectrum of BSE energies, the energy losses (plasmon losses) which become observable in reflection at lower primary energies $E > 10$ keV, the Auger electron spectrum and the fine structure of the SE energy spectrum. Of special interest in semiconductor technology are electron spectrometers which can measure the local surface potential (see e.g. Balk et al. 1976). Surely all these possibilities cannot be realized by a single electron spectrometer, but this will be an interesting field for future developments.

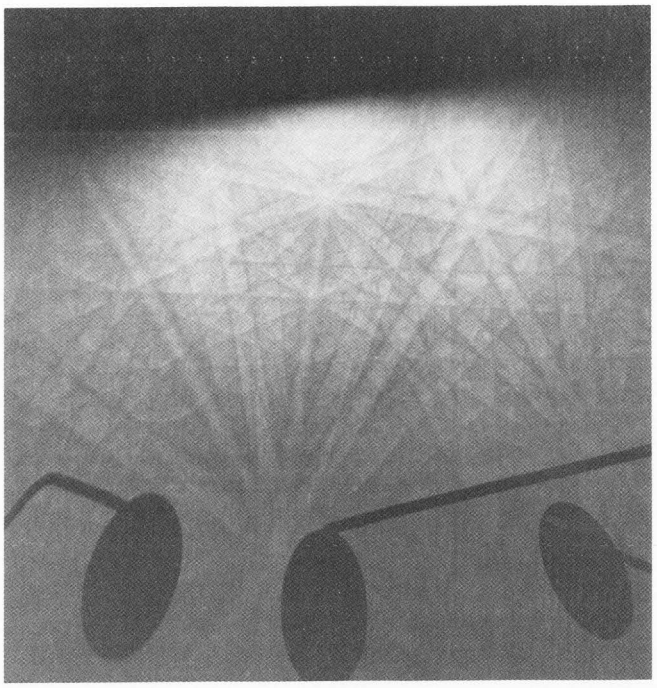

Fig. 9. EBSP of a platinum specimen at E = 40 keV recorded directly on a photographic emulsion inside an SEM.

SIGNAL PROCESSING

Detector strategy cannot be seen isolated without discussing possibilities of analogue or digital image processing. The normal analogue signal processing of the video signal U_v

$$U_v' = (a\,U_v - b)^{1/\gamma} + c\,dU_v/dt \qquad (7)$$

is incorporated in most SEMs. The signal mixing A + B or A – B of two detectors as discussed for SE and BSE can be realized by a simple operation amplifier. Two signals A, B or A – B, A + B can be observed simultaneously if two video tubes are available. Another possibility is the on-line integration of the SE signal as discussed in *Reconstruction of surface topography* above.

However, digital image storing and processing will be more flexible. E.g. for recording an A – B signal it will be necessary to use equal mean signal amplitudes of A and B and a correct value of the additive signal C. If the signals A and B are stored digitally the mean signal amplitudes can be equalized by computation. By knowing the dependence of the signal of a multi-detector system on the material and surface-normal orientation ($\overline{Z}$, Φ, χ) the calculation of these quantities can be done even for more complicated analytical laws. E.g. the signal of an Si(Li) x-ray detector can be read and the knowledge of $\overline{\eta}$, Φ and χ allows one to apply a ZAF correc-

tion for tilted surface elements (Love et al. 1978, Lödding and Reimer 1978, Love and Scott 1981).

Furthermore, all standard methods of image processing, e.g. stereology, one- and two-dimensional gradient, Laplace-transformation etc., can be applied. A feed-back to the lens current can be applied to record a surface profile by automatic focusing (Holburn and Smith 1979). The storage of two micrographs as a stereo-pair allows one to use stereometry automatically. Stereometry can only be applied if there are features in the micrographs which show a parallax but not if there is no fine structure at a flat or curved surface. The described methods to get Φ and χ from the $A-B$ and $A+B$ signals can complete the information which is missed in stereometry.

A recording of material and surface topography as e.g. in Fig. 3 for different primary electron energies or the use of high-pass BSE energy filtering with a variable lower threshold can be used to reconstruct the three-dimensional internal structure of the specimen with the knowledge of the electron penetration and beam broadening.

These are only a few examples to demonstrate that a computer fed with basic laws about electron-specimen interactions can complete a detector strategy.

REFERENCES

Balk LJ, Feuerbaum HP, Kubalek E, and Menzel E. (1976). Quantitative voltage contrast at high frequencies in the SEM, Scanning Electron Microsc. 1976; I: 615-624, 646.

Banbury JR and Nixon WC. (1969). A high contrast directional detector for the SEM. J. Phys. **E 2**, 1055-1059.

Baumann W and Reimer L. (1981). Comparison of the noise of different electron detection systems using a scintillator-photomultiplier combination. Scanning **4**, 141-151.

Blaschke R. and Schur K. (1972). Der Informationsgehalt des Rückstreubildes im Raster-Elektronenmikroskop. (Information of micrographs recorded by backscattered electrons.) Beitr. elektr. mikr. Direktabb. Oberfl. **5**, 33-52, Remy Münster.

Booker GR. (1970). Scanning electron microscopy, electron channelling effects, in: Modern Diffraction and Imaging Techniques in Material Science, S. Amelinckx (ed.), p. 613-653, North-Holland Publ. Co., Amsterdam-London.

Castaing R. (1960). Electron probe microanalysis. Adv.-Electr.-Electr. Phys. **13**, 317-386.

Drescher H, Reimer L, and Seidel H. (1970). Rückstreukoeffizient und Sekundärelektronenausbeute von 10-100 keV-Elektronen und Beziehungen zur Raster-Elektronenmikroskopie. (Backscattering coefficient and secondary electron yield of 10-100 keV electrons and relations to SEM.) Z. angew. Phys. **29**, 331-336.

Drescher H, Krefting ER, Reimer L, and Seidel H. (1974). The orientation dependence of the electron backscattering coefficient of gold single crystal films. Z. Naturforschg. **29a**, 833-837.

Gentsch P and Reimer L. (1972). Messungen zum magnetischen Kontrast im Raster-Elektronenmikroskop. (Measurements of type I magnetic contrast in SEM.) Beitr. elektr. mikr. Direktabb. Oberfl. **5**, 299-312, Remy, Münster.

Griffiths BW, Pollard P, and Venables JA. (1972). A channel plate detector for the scanning electron microscope. Proc. 5th European Congr. Electron Microscopy 1972, p. 176-177, The Institute of Physics, London-Bristol.

Hoffmann M and Reimer L. (1981). Channelling contrast on metal surfaces after ion beam etching. Scanning **4**, 91-93.

Holburn DM and Smith KCA. (1979). On-line topographic analysis in the SEM, Scanning Electron Microsc. 1979; II: 47-52.

Kimoto S, Hashimoto H, and Suganuma T. (1966). Stereoscopic observation in scanning microscopy using multiple detectors, in: The Electron Microprobe, T.D. McKinley, K.F.J. Heinrich, and D.B. Wittry (eds.), p. 480-489, John-Wiley & Sons, New York.

Lebiedzik J. (1979). An automatic topographical surface reconstruction in the SEM. Scanning **2**, 230-237.

Lebiedzik J and White EW. (1975). Multiple detector method for quantitative determination of microtopography in the SEM, Scanning Electron Microsc. 1975; 181-188.

Lödding B and Reimer L. (1978). Energy dispersive x-ray microanalysis on tilted specimens using a modified ZAF correction. Scanning **1**, 225-229.

Love G, Cox MG, and Scott VD. (1978). A versatile atomic number correction for electron-probe microanalysis. J. Phys. **D 11**, 7-21.

Love G and Scott VD. (1981). Updating correction procedures in quantitative electron-probe microanalysis. Scanning **4**, 111-130.

Moll SH, Healey F, Sullivan B, and Johnson W. (1978). A high efficiency, non-directional backscattered electron detection mode for SEM, Scanning Electron Microsc. 1978; I: 303-310.

Morin R, Pitaval M, Besnard D, and Fontain G. (1979). Electron channelling imaging in scanning electron microscopy. Phil. Mag. **A 40**, 511-524.

Niedrig H. (1978). Physical background of electron backscattering. Scanning **1**, 17-34.

Reimer L. (1973). Contrast in the different modes of SEM, in: Scanning Electron Microscopy: systems and applications, W.C. Nixon (ed.), p. 120-125, The Inst. of Physics, London-Bristol.

Reimer L. (1979). Electron-specimen interactions, Scanning Electron Microsc. 1979; II: 111-123.

Reimer L and Drescher H. (1977). Secondary electron emission of 10-100 keV electrons from transparent films of Al and Au. J. Phys. **D 10**, 805-815.

Reimer L and Volbert B. (1979). Detector system for backscattered electrons by conversion to secondary electrons. Scanning **2**, 238-248.

Reimer L and Volbert B. (1980a). New detector system for conversion of backscattered to secondary electrons. Inst. Phys. Conf. Ser. No. 52, 89-92. The Inst. of Physics, London-Bristol.

Reimer L and Volbert B. (1980b). Separation of topographic and material contrast in SEM by different detection systems. Electron Microscopy 1980, Vol. 3, 172-173, The Hague, 7th European Congr. on Electron Microscopy Foundation, Leiden.

Reimer L, Badde HG, Seidel H, and Bühring W. (1971). Orientierungsanisotropie des Rückstreukoeffizienten und der Sekundärelektronenausbeute von 10-100 keV-Elektronen. (Orientation anisotropy of the backscattering coefficient and the secondary electron yield of 10-100 keV electrons.) Z. angew. Phys. **31**, 145-151.

Reimer L, Pöpper W, and Bröcker W. (1978). Experiments with a small solid angle detector for BSE, Scanning Electron Microsc. 1978; I: 705-710.

Reimer L and Tollkamp C. (1980). Measuring the backscattering coefficient and secondary electron yield inside a SEM. Scanning **3**, 35-39.

Robinson VNE. (1975). Backscattered electron imaging, Scanning Electron Microsc. 1975; 51-60, 92.

Venables JA and Harland CJ. (1973). Electron back-scattering patterns – a new technique for obtaining crystallographic information in the SEM. Phil. Mag. **27**, 1193-1200.

Venables JA, Griffiths BW, Harland CJ, and Ecker KH. (1974). Some developments in SEM instrumentation. Rev. Phys. Appl. **9**, 419-425.

Venables JA and bin-Jaya R. (1977). Accurate microcrystallography using electron back-scattering patterns. Phil. Mag. **35**, 1317-1332.

Volbert B. (1981). Verbesserung der topographischen Information durch Überlagerung von Sekundärelektronen (SE)-und invertierten Rückstreuelektronen (BSE)-Signal. (Improvement of topographic information by superposition of SE and BSE signals.) Beitr. elektr. mikr. Direktabb. Oberfl. **14**, 325-330, Remy, Münster.

Volbert B and Reimer L. (1980). Advantages of two opposite Everhart-Thornley detectors in SEM, Scanning Electron Microsc. 1980; IV: 1-10.

Walker AR and Booker GR. (1976). A simple energy filtering backscattered electron detector, in: Developments in Electron Microscopy and Analysis, p. 119-122, Academic Press, London-New York-San Francisco.

Wells OC. (1971). Low-loss image for scanning electron microscopy. Appl. Phys. Letters **19**, 232-235.

Wells OC. (1972). Explanation of the low-loss image in the SEM in terms of electron scattering theory, Scanning Electron Microsc. 1972; 169-176.

Wells OC. (1974). Scanning Electron Microscopy, p. 133, McGraw-Hill, New York.

Wells OC. (1978). Effect of collector position on type-2 magnetic contrast, Scanning Electron Microsc. 1978; I: 293-298.

Wells OC. (1979). Effects of collector take-off angle and energy filtering in the BSE image in the SEM. Scanning **2**, 199-216.